Supplementary Information

New thermoplastic poly(ester-ether) elastomer with enhanced mechanical properties derived from long-chain dicarboxylic acid for medical device applications

Xiangwei Wu [a], Tao Yang [b], Xiaoqin Jiang [b], Wei Su [a], Fei Liu [b*], Jinggang Wang [b], Jin Zhu[b]

a. The First Affiliated Hospital of Ningbo University, Ningbo, Zhejiang 315020, China

b. Key Laboratory of Bio-based Polymeric Materials Technology and Application of Zhejiang Province, Ningbo Institute of Materials Technology and Engineering, Chinese Academy of Sciences, 1219 Zhongguan West Road, Zhenhai, Ningbo, Zhejiang, 315201, China.

* Corresponding Authors:

Dr. Fei Liu, liufei@nimte.ac.cn

Supporting Information

Number of Pages	9 (S1-S9)
Number of Figures	5 (Figure S1-S5)
Number of Tables	4 (Table S1-S4)

Sample treatment

All samples were heat-pressed for 10 minutes at a melting point of 20 ^{o}C above PPThF-PTMEGs through a flat-plate vulcanizer (10 MPa), and the light-colored films were removed with liquid nitrogen, which is 100 mm (length) × 100 mm (neck width) × 1.0 mm (thickness).

Characterization

Viability Assay (MTS). Cell viability: a colorimetric method employing a novel tetrazolium compound, [3-(4,5-dimethylthiazol-2-yl)-5-(3-carboxymethoxyphenyl)-2-(4-sulfophenyl)-2H-tetrazolium, inner salt], in conjunction with an electron coupling reagent, phenazine methosulfate (PMS). Viable cells reduce MTS to a water-soluble formazan product, the absorbance of which is quantifiable at 490 nm. This reduction is catalyzed by dehydrogenase enzymes present in metabolically active cells, with the resulting formazan concentration being directly proportional to cell viability. At each specified time point (1, 3, and 5 days), the culture medium was removed, and MTS solution was added to the samples. After a 4-hour incubation, the UV-visible absorbance at 490 nm was measured. Polystyrene plates served as controls for the assay.

Cell Morphology; Cell morphology on both control and polymeric films was evaluated using fluorescence microscopy at 10× magnification. Following incubation periods of 1, 3, and 5 days, cells were fixed in 4% formaldehyde for 60 min at RT. After rinsing with PBS, cells were incubated with phalloidin-tetramethyl rhodamine conjugate for 45 mins at 37 °C in the dark. Nuclear staining was performed using 4',6-diamidino-2-phenylindole. Cells cultured on glass coverslips in 24-well plates served as controls.

Statistical Analyses; Cell viability assays were conducted in triplicate. Data are presented as mean values ± standard deviation. Statistical significance was evaluated using Student's t-test, with ** indicating $P \leq 0.01$.

SAXS and WAXS measurements. The crystallinity (χ_c) was calculated through WAXS-peak-differentiation-imitating analysis.

$$Crystallinity\left(\chi_{c,h}\right)=\frac{\sum A_{crystalline(c,h)}}{\sum A_{crystalline(c,h)}+A_{amorphous}}\times 100\%=\frac{1\text{-}A_{amorphous}}{\sum A_{crystalline(c,h)}+A_{amorphous}}$$

$$Crystallinity\left(\chi_{c,s}\right)=\frac{\sum A_{crystalline(c,s)}}{\sum A_{crystalline(c,s)}+A_{amorphous}}\times 100\%=\frac{1\text{-}A_{amorphous}}{\sum A_{crystalline(c,s)}+A_{amorphous}}$$

1. Supplementary Figures

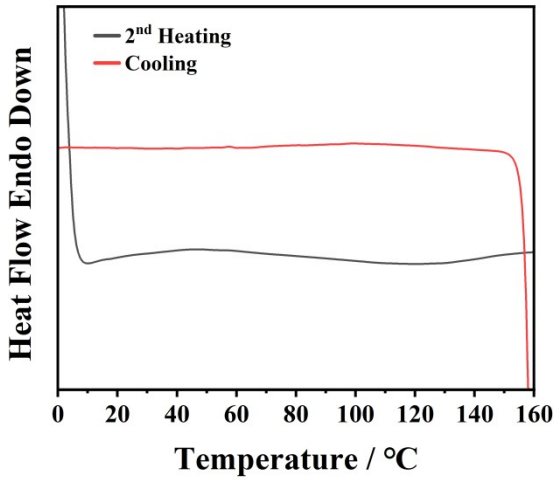

Figure S1. DSC curves of cooling and the second heating scans of PVC.

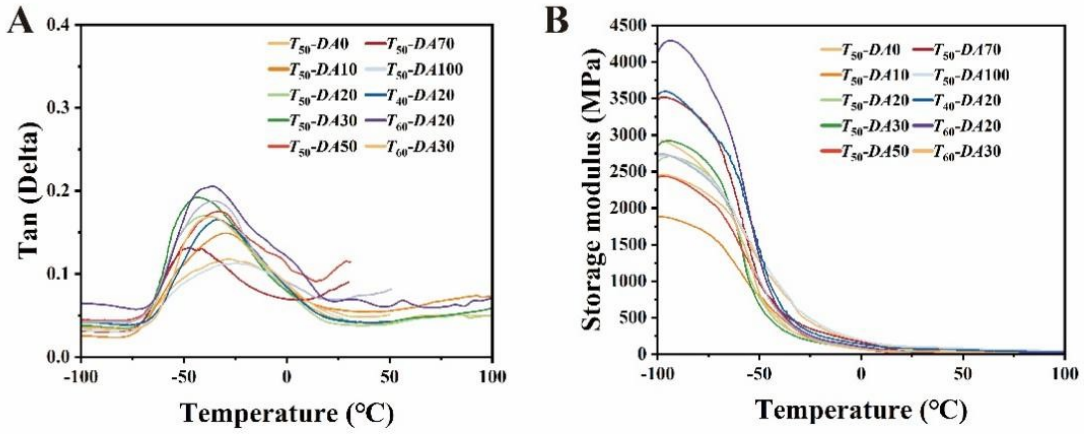

Figure S2. Tan δ (a) and storage modulus (b) as a function of temperature for T_x-*DA*ys.

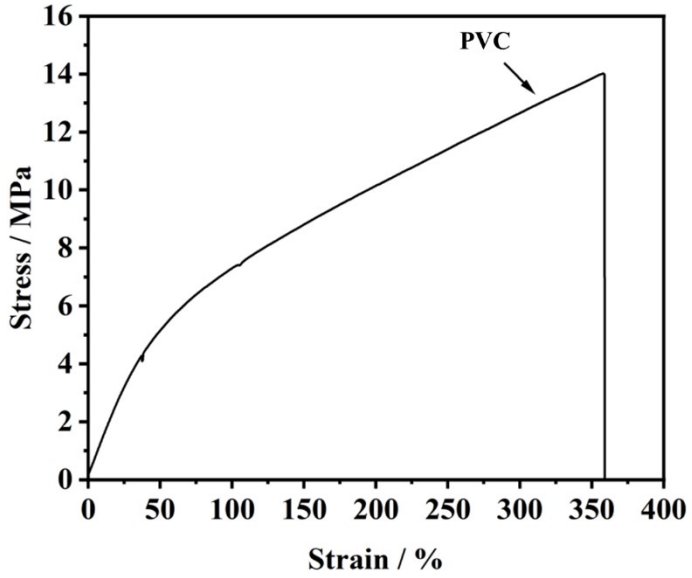

Figure S3. Stress-strain curves for PVC.

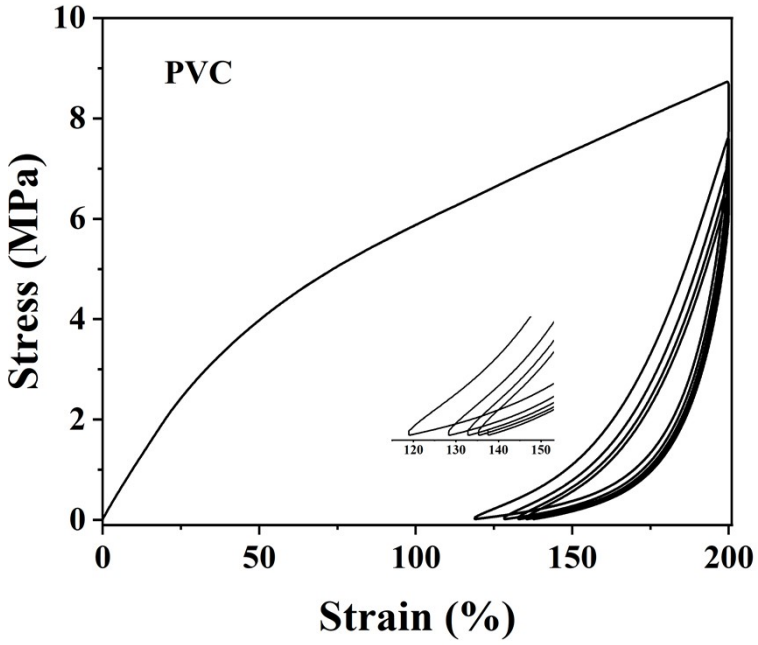

Figure S4. Cyclic tensile testing curves at 200% strain for PVC.

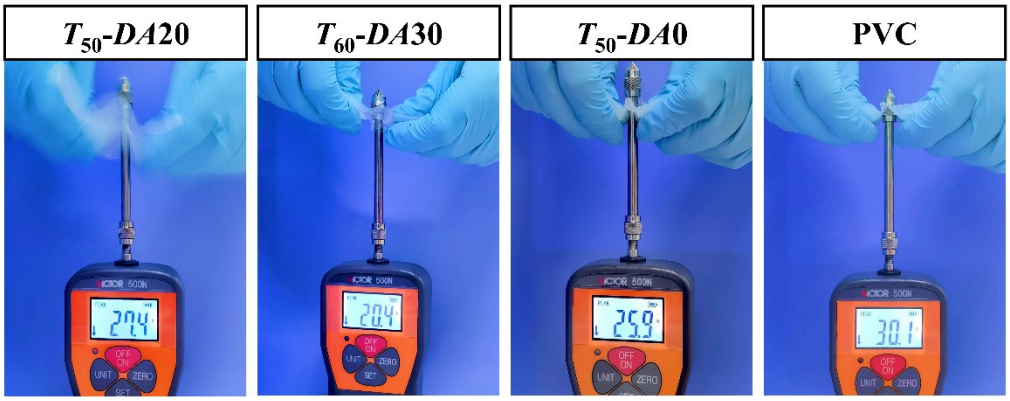

Figure S5. Puncture test for T_x-*DA*y samples and PVC.

2. Supplementary Tables

Table S1. Feeding Ratios and Reaction Conditions in T_x-*DA*ys

Sample	Feeding ratios (mol %)				1st step		2nd step	
	DMT	BDO	PTMEG	DA	*T* (℃)	*t* (h)	*T* (℃)	*t* (h)
T_{50}-*DA*0	38.43	57.52	4.05	0	200	4	250	5
T_{50}-*DA*10	37.50	53.83	4.46	4.21	200	4	240	4
T_{50}-*DA*20	33.33	53.83	4.54	8.30	220	5	240	4
T_{50}-*DA*30	29.19	53.76	4.49	12.55	180	5	250	4
T_{50}-*DA*50	20.87	53.62	4.64	20.87	190	5	240	5
T_{50}-*DA*70	12.54	53.52	4.79	29.15	180	4	230	5
T_{50}-*DA*100	0	53.32	5.02	41.65	180	4	250	4
T_{40}-*DA*20	33.33	55.22	3.14	8.31	190	5	250	4
T_{60}-*DA*20	29.14	55.20	3.20	12.46	180	5	250	4
T_{40}-*DA*30	32.00	53.93	6.07	8.00	180	5	240	5
T_{60}-*DA*30	27.97	53.83	6.17	12.03	190	5	240	4

Table S2. L, L_c and L_a values of T_x-*DA*y samples after annealing

Sample	χ_c (%) [a]	q^* (Å)	Long period (nm)		
			L	L_c	L_a
T_{50}-*DA*0	30.6	0.047	13.4	4.1	9.3
T_{50}-*DA*10	22.4	0.042	15.0	3.4	11.6
T_{50}-*DA*20	20.4	0.038	16.5	3.3	13.2
T_{50}-*DA*30	12.6	0.034	18.8	2.4	16.7
T_{50}-*DA*50	8.7	0.032	19.6	1.7	17.9
T_{50}-*DA*70	21.7	0.031	20.2	4.4	15.8
T_{50}*DA*100	34.2	0.033	19.0	6.5	12.5
T_{40}-*DA*20	23.6	0.039	16.1	3.8	12.3
T_{60}-*DA*20	15.5	0.028	22.4	3.5	18.9
T_{40}-*DA*30	16.4	0.032	19.6	3.2	16.4
T_{60}-*DA*30	12.3	0.036	17.5	2.2	15.3

[a] The crystallinity (χ_c) was calculated through WAXS-peak-differentiation-imitating analysis.

Table S3. Elastic properties of T_x-*DA*y[a]

Sample	η_{r1} (%)	η_{r2} (%)	η_{r3} (%)	η_{r4} (%)	η_{r5} (%)
T_{50}-*DA*0	34.8±0.7	94.8±0.7	96.7±0.8	97.9±0.6	98.3±0.3
T_{50}-*DA*10	45.4±6.9	95.9±0.1	98.4±1.7	99.1±1.0	99.9±0.8
T_{50}-*DA*20	58.6±0.4	97.5±0.3	98.1±0.1	99.5±0.1	99.5±0.1
T_{50}-*DA*30	59.6±1.8	96.9±0.5	98.2±0.4	98.6±0.2	99.6±0.2
T_{50}-*DA*50	65.3±0.6	95.7±0.1	96.9±1.6	97.0±1.4	97.4±2.0
T_{50}-*DA*70	38.0±0.1	95.5±0.3	95.4±1.0	95.7±1.4	97.6±1.3
T_{50}*DA*100	16.6±0.1	93.2±0.3	96.3±0.1	97.1±0.2	98.2±0.1
T_{40}-*DA*20	34.4±0.8	96.3±0.1	97.5±0.1	98.7±0.4	99.0±0.2
T_{60}-*DA*20	60.3±3.8	96.8±0.4	98.2±0.1	98.9±0.3	99.4±0.4
T_{40}-*DA*30	59.2±2.0	95.4±0.6	97.5±0.1	98.4±0.2	99.1±0.1
T_{60}-*DA*30	69.0±0.7	96.9±0.1	98.3±0.1	99.0±0.2	99.4±0.2

[a] Shape recovery ratio at 200% strain using cyclic tensile test demonstrates elastic property.

Table S4. The thermal stability evaluation

Specimens	$T_{d,5\%}$ (°C)	$T_{d,50\%}$ (°C)	$T_{d,max}$ (°C)	R_{600} (wt%)	T_g (°C)
T_{50}-*DA*0	379	409	408	1.1	-25.1
T_{50}-*DA*10	360	409	403	1.2	-27.8
T_{50}-*DA*20	375	411	407	1.4	-38.6
T_{50}-*DA*30	374	413	405	2.6	-41.6
T_{50}-*DA*50	374	415	404	3.1	-47.6
T_{50}-*DA*70	368	409	403	4.2	-51.2
T_{50}-*DA*100	375	407	404	6.2	-22.4
T_{40}-*DA*20	372	412	405	1.4	-30.1
T_{60}-*DA*20	374	416	408	1.2	-40.2
T_{40}-*DA*30	372	407	403	2.7	-32.6
T_{60}-*DA*30	373	408	409	1.9	-42.6